Existence of Water Droplets at Liquid/Air Interfaces

Supplementary Methods Part 1: Description of experimental apparatus and procedure

Three experimental configurations were constructed to observe the existence and behaviour of water droplets at solvent surfaces. The first two rely on dosing water by means of condensation from a humid environment, whereas the third relies on manual dosing of droplets to the solvent-air interface. In all cases, the droplets are observed using the upright, Olympus BX51M optical microscope with the reflected light mode. For contact angle measurements, images are recorded at x50 magnification using the Olympus XM10 1.4 megapixel CCD camera and image calibration is performed using a reference grid. When dosing water droplets by condensation, different substrates and chambers were developed to optimise image capturing as required. However, the fundamental process is (i) humidifying a flow of nitrogen, (ii) delivering it to the solvent-air interface and (iii) ensuring the local temperature remains below the saturation temperature for the vapour flow to drive water condensation.

As indicated in Fig. S1 a source of dry, filtered nitrogen is split into two streams. The first is directed to a system of flow meters and controllers, Fig. S1a, the second towards a wash bottle containing de-ionised and filtered water at 60°C, Fig. S1b. The two flows are combined at controlled proportions and pass through a final meter to monitor the total flow rate. This total flow is maintained at approximately $1-1.5\ \mathrm{L\ min^{-1}}$. The relative humidity is measured in each experimental arrangement using the Rotronic HygroLog NT2-D and the HygroClip SC05 humidity probe.

For the first experimental setup, indicated in Fig. S1(c), the flow is directed to a glass well containing the solvent of interest. This occurs either by the indicated method of filling a chamber with the supply of humid vapour or alternatively by delivering the flow through a wide nozzle across the surface of the solvent. The glass well is approximately 5 mm deep, formed by adhering a thin section of glass tube to an inverted chambered Lab-Tek cover slip. The chamber is filled with ice to maintain a chilled solvent to induce water condensation while reducing solvent evaporation and convection currents. This experiment was carried out on a lab bench with a portable extractor/filter positioned to remove the solvent vapours. Prior to each experimental run, dry nitrogen is guided to flow over the substrate to avoid condensation onto the glass surfaces.

The second experimental setup, shown in Fig. S1d, uses a flow chamber (Fig. S1e), constructed using the Eden250™ 3D Printing System. There is an inlet in the chamber for the humid flow of nitrogen, which passes over the substrate, solvent and the humidity probe before exiting at the far end. There is also a holder to fix the humidity probe while minimising flow disruption. A microscope coverslip, cleaned as per the protocol discussed later in this section, is placed on top of two glass slides to reduce the distance to the microscope lens and allow imaging from the open port in the chamber. Once the glass substrate is in place, dry nitrogen flows across the sample to ensure minimal water condensation prior to solvent dosing.

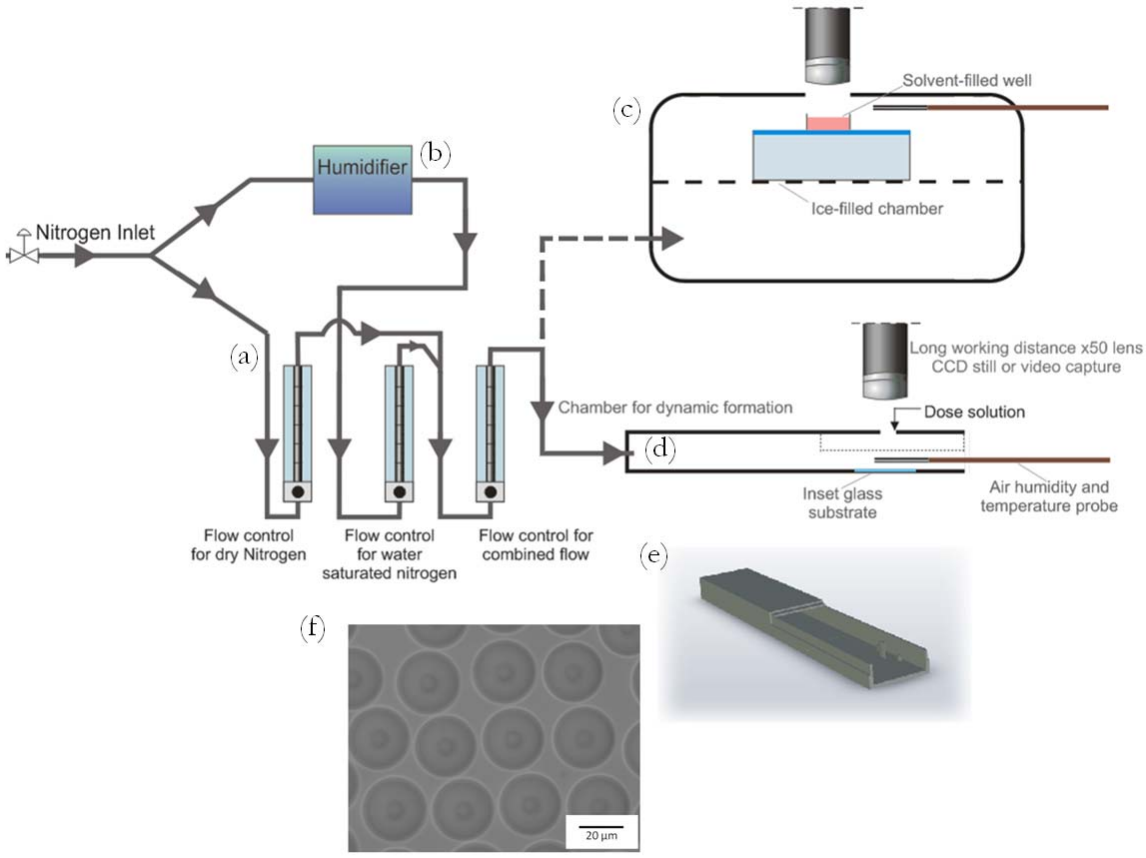

FIG. S1. Apparatus for the delivery and observation of water condensate at a liquid/air interface to allow droplet contact angle measurement. (a) controls the proportion of humid and dry nitrogen delivered to the chamber, (b) humidifies a flow of nitrogen, (c) shows the glass well containing the solvent of interest in the humidity chamber, (d) shows the flow chamber technique, (e) is a model of the flow chamber used, and (f) condensed water droplets at toluene-air interface, as imaged using this apparatus.

The solvent is dosed using a micropipette through the open port. Normally the solvent dose volume is 60 – 100 µL. For toluene, its slow evaporation provides sufficient cooling to induce condensation once at a high humidity (>80%), without driving rapid droplet movement; FIG. S1f. With other solvents either slow evaporation does not induce sufficient cooling to drive water condensation (e.g. butyl acetate) or alternatively rapid evaporation (e.g. chloroform) leads to total solvent loss within too short a period for observation and a rapid movement of water droplets. To avoid these problems, the solution is cooled to between 5 and 13 °C. This was achieved initially through packing the chamber in ice and pre-chilling the solvent. Due to heat from the environment remaining quite constant, this maintained the glass cover slip at 12-13 °C for the duration of an experiment. This technique was replaced later, with cooling provided to the chamber by means of a Peltier element. The temperature of the substrate was maintained at approximately 5-10 °C.

The third experimental setup incorporates the additional components shown in Fig. S2. This figure shows a glass capillary tip formed using a Narishige PC-10 vertical heating/pulling system. The final internal diameter of the capillary is approximately 500 nm. This is connected via tubing to a 1 mL syringe, filled with Nanopure (Thermo Scientific 18MΩ) de-ionised water. The glass tip is mounted on the Kleindiek MM3A-EM nanomanipulator (b). The combination of a micromanipulator with an ultrafine tip allows for careful positioning and dosing of nanolitre quantities of fluid to the solvent-air interface. The water droplets have been dosed and studied in both the solvent well and flow chamber experimental configurations discussed earlier.

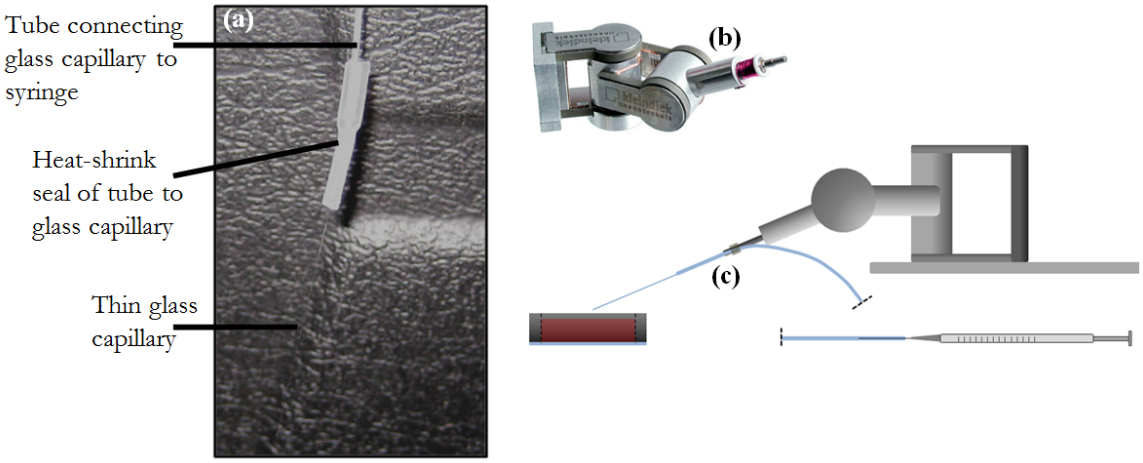

FIG. S2. A glass capillary shown in (a) is attached to a Kleindiek micromanipulator (b) and used as shown in (c) to dose water from a syringe to the solvent/air interface.

In all cases, the microscope views the droplets from above, as indicated in Fig. S3a. An example video recording of the observed droplets on a butyl acetate interface is included in the Supplementary Information. When focusing close to the centre of a droplet, the submerged radius R is quite clear, with the outer edge of the dark, sharp black line taken to be the outer edge of the droplet as seen in Fig. S3b. Re-focusing towards the top of the droplet reveals a dark circle at the solvent surface. This is understood to be the portion of the droplet emerging from the solvent and the associated three phase contact line and is also shown in Fig. S3b. From this the three phase contact radius, r, is measured. Calibrating the microscope with an AFM calibration grid, the CCD images captured can be used with image analysis software, ImageJ [20], to extract the measurements required. Where the contrast is sufficient a threshold is applied, converting the selected image to a binary format. The outer and three phase contact diameters are detected using a built-in particle counting technique. Where the contrast is not sufficient, which is true for most cases, manual measurements are taken instead. Two circles are fitted to each droplet, showing the outer diameter and three phase contact diameter. The relationship in Eq. (S1) is a simple geometric equation that allows the contact angle to be calculated:

$$\sin\theta = \frac{r}{R} . \qquad \text{(S1)}$$

It is important to maintain clean apparatus to ensure accurate contact angle and surface tension measurements. Vials for storing the solvent prior to dosing were (i) soaked in a potassium chloride/propan-2-one mix and then cleaned by sequential steps of rinsing and sonication in (i) HPLC grade acetone, (ii) HPLC grade propan-2-one and (iii) de-ionised water. Initial drying was carried out with high-pressure nitrogen and further drying was completed using an oven at 110 °C. When using glass coverslips, watch glasses or glass wells they were washed in soapy water, rinsed thoroughly in de-ionised water and then sonicated and rinsed in (i) HPLC grade acetone, (ii) HPLC grade propan-2-one, (iii) deionised water followed by high pressure nitrogen drying. A final step prior to use was an exposure to an oxygen plasma for 6 minutes using a Diener Pico Plasma Cleaner.

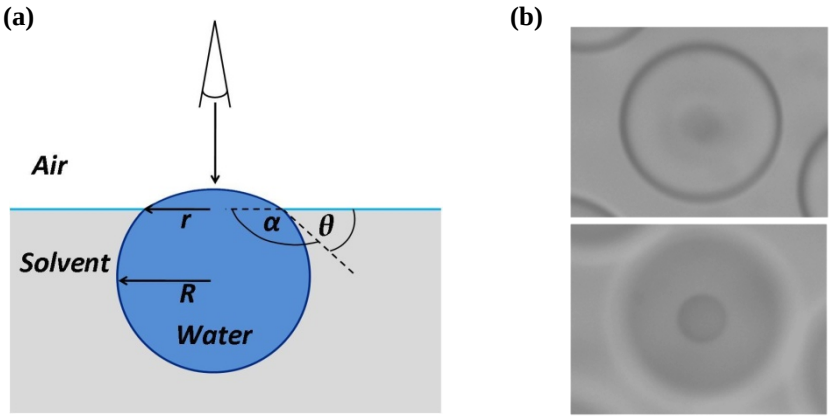

FIG. S3. (a) Illustrates the positioning of a water droplet at a solvent/air interface and indicates the key geometrical measurements, the radius of curvature of the submerged droplet (R), the radius *r* of the three phase contact region and the contact angle, θ. (b) Shows a pair of images taken of a water droplet at a butyl acetate-air interface, with optical microscopy. This technique allows focusing on and measurement of both *R* and *r*.

Supplementary Methods Part 2: Validation of method to measure contact angles by optical microscopy

(i) Contact angle and radius measurement

The use of optical analysis to measure both the three phase contact radius and the total droplet radius of water droplets almost completely submerged in a solvent has not previously been reported as far as we are aware. However, a number of reports take advantage of similar observations.

Mingins and Scheludko [17] looked at the change in wetting angles of glass microspheres with inclusion of different levels of surfactants. The method observed the glass particles trapped at the end of pendant drops of water using an inverted optical microscope. According to the authors, when a three phase contact is formed, the portion of the spherical particle that projects from the liquid strongly scatters light reflected from it, resulting in a black disc corresponding to the three phase contact wetting perimeter. An outline of the submerged droplet is also visible.

Each of their subsequent papers includes an examination of the equilibrium receding contact angle of spherical particles with the electrolyte [21, 22] using the same technique. This technique and its results are referenced and used by Amirfazli *et al*. [23] and Aveyard *et al*. [4, 24].

(ii) Confirmation with alternative technique

An additional validation was carried out by examining the interference rings produced at the thin liquid wedge close to the three phase interaction zone between the water droplet and the solvent-air interface, similar to Stockelhuber *et al* [15]. These rings can be seen in Fig. S4a. The intensity of the grey values are identified by ImageJ [20] and mapped across the diameter of the region, as shown in Fig. S4b. The depth of the liquid wedge can be estimated at each ring using an estimate for the

wavelength based on the known mercury lamp spectral peak of 578nm and the Eq. (S2):

$$a_i = \frac{i\lambda}{2n_{fl}}, \tag{S2}$$

where a_i is the depth at the i-th fringe when observed with light of wavelength λ using a fluid of refractive index, n_{fl}. A manually fit circle to the data points (Fig. S4c) shows approximately 165° contact angle for a water droplet at a toluene-air interface, which is consistent with values found using the method of Mingins and Scheludko [17].

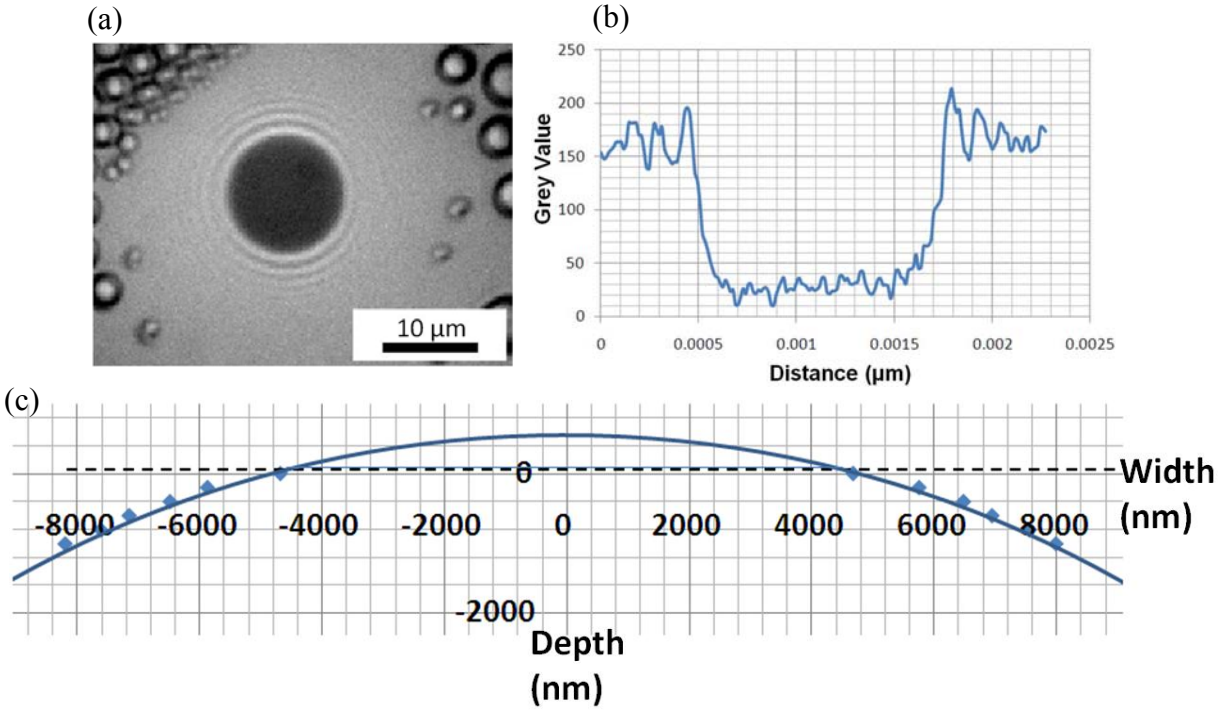

FIG. S4. (a) An interference pattern around the three phase contact line, (b) the associated grey intensity values across the diameter of the pattern and (c) a manual fit of depth data from interference measurements.

(iv) Validation by error analysis

The errors involved in the measurement of the three phase contact radius are examined using butyl acetate as the solvent. The values vary from 0.98% of the radius value for extremely large drops to 5.7% of the radius value for smaller droplets. This will increase further with decreases in droplet size due to the resolution of the camera and the stability of the droplets. The measurement of the diameter is limited not only by the manual focus but also by the pixilation of the image. We looked at the region of ambiguity in each image and measured the maximum and minimum interpretable drop sizes in a selection of 20 droplets from different experimental runs.

A similar technique applied to the total droplet diameter measurement, measured from the edge of the outer dark rim, which is observable only when focusing down through the droplet to the widest point. The error in measurement for water droplets at butyl acetate surfaces varies from 0.27% of the radius value for extremely large drops to 6.7% of the radius value for smaller droplets. At the worst case, combining the errors of both measurements, the error in contact angle for smaller droplets is ±1° in this case. This is expected to decrease for larger droplets due to the resolution of the microscope, and indeed was recorded here as ±0.36°. Small droplets are therefore expected to have much larger errors

associated with them due to the method of measurement.

Supplementary Methods Part 3: Details of surface tension balance and assumptions

We examine the wettability of a liquid droplet at a solvent-air interface using a surface tension balance approach derived in detail by Pujado & Scriven [25] and then adopted by other groups active in the analysis of liquid lenses. The level of projection of the droplet into each phase is determined by the relative wettability and leads to an equilibrium shape made up of two spherical caps, as seen in Fig. S5.

FIG. S5. Two dimensional representation of a water droplet at a solvent-air interface, showing the forces acting on the droplet.

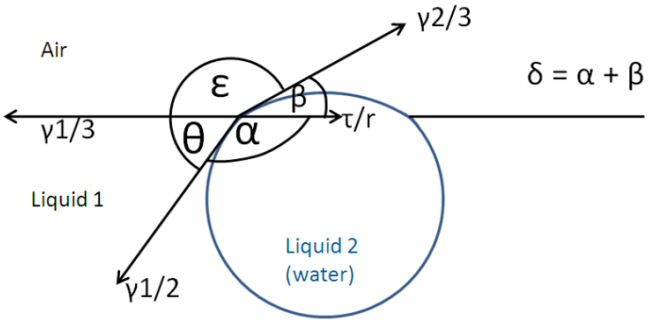

When the forces acting at the interfaces identified in Fig. S5 are resolved, they include a term for the three phase line tension and yield the following relationships for the angles of the droplet:

$$\alpha = \cos^{-1}\left(\frac{\gamma_{1/2}^2 - \gamma_{2/3}^2 + \left(\gamma_{1/3} - \frac{\tau}{r}\right)^2}{2\gamma_{1/2}\left(\gamma_{1/3} - \frac{\tau}{r}\right)}\right), \quad \beta = \cos^{-1}\left(\frac{\gamma_{2/3}^2 - \gamma_{1/2}^2 + \left(\gamma_{1/3} - \frac{\tau}{r}\right)^2}{2\gamma_{2/3}\left(\gamma_{1/3} - \frac{\tau}{r}\right)}\right), \tag{S3}$$

where $\gamma_{2/3}$, $\gamma_{1/2}$, $\gamma_{1/3}$ are the surface tensions of the air-water, solvent-water and air-solvent interfaces, respectively, τ is the line tension and r is the radius of the three phase contact region of the droplet. If in these equations the line tension is allowed to reach zero, then the remaining relationships are those found when considering the Neumann triangle.

These relationships are all that is required to analyse and predict the behaviour of a pure three phase liquid-liquid-vapour system. However, to legitimately apply this model, the following must be assumed:

- The solvent surface is planar up to the droplet interface.
- Gravity does not have any significant effect on the droplets. This was tested by looking at the capillary length, as defined by Adamson *et al*. [13],

$$a = \sqrt{\frac{\gamma}{g\Delta\rho}} \tag{S4}$$

where γ is the surface tension, $\Delta\rho$ is the difference in density between the droplet in question and its surroundings, g is the acceleration due to gravity. For a droplet of water in air the resultant capillary length is 2.7 mm and the smallest capillary length for solvents used in this thesis is 2.4 mm. The largest of the drops analysed was approximately 0.4 mm in diameter but the bulk of analysis was carried out on drops in the tens of micrometers scale.

- Bulk surface tensions are independent of drop size for the scale of drops examined.
- The system is at chemical and thermal equilibrium.

Supplementary Methods Part 4: Mutual Partial Solubility

The mutual partial solubility of chloroform, butyl acetate and toluene is noted within the manuscript. The measured solubilities are provided in Table S1, as reported by Donohue et al. [7].

Solvent	Mole fraction water	Mole fraction organic
Chloroform	0.0050	0.0012
Butyl Acetate	0.0745	0.00995
Toluene	0.0025	0.00010

TABLE S1. Mutual solubility data for three organic solvents used within this study, as reported by Donohue et al. [7].

Supplementary Videos: A video has been provided showing the packing of water droplets at a butyl acetate/air interface using the set-up described in this letter.

Supplementary References

20. Rasband, W. S., U. S. National Institutes of Health, Bethesda, Maryland, USA. http://rsb.info.nih.gov/ij/.
21. Alexandrova, L., Rao, K. H., Forsberg, K. S. E., Grigorov, L. & Pugh, R. J. Three-phase contact parameters measurements for silica-mixed cationic–anionic surfactant systems. *Coll. Surf. A 2009*, 348, 228-233.

22. Nguyen, A. V., Alexandrova, L., Grigorov, L. & Jameson, G. J. Dewetting kinetics on silica substrates: Three phase contact expansion measurements for aqueous dodecylammonium chloride films. *Min. Eng*., 19, 2006, 651-658.

23. Amirfazli, A. & Neumann, A. W. Status of the three-phase line tension. *Adv. Coll. Int. Sci.*, 2004, 110, 121-141.

24. R. Aveyard, J. H. C. D. N. Small solid particles and liquid lenses at fluid/fluid interfaces. *Coll. Poly. Sci.*, 2000, 278, 155-163.

25. Pujado, P. R. & Scriven, L. E. Sessile Lenticular Configurations: Translationally and Rotationally Symmetric Lenses. *J. Coll. Int. Sci.*, 1972, 40, 82-98.